Clavulanic Acid Dehydrogenase: Structural and Biochemical Analysis of the Final Step in the Biosynthesis of the β-Lactamase Inhibitor Clavulanic Acid[†,‡]

Alasdair K. MacKenzie,[§,||] Nadia J. Kershaw,[§,⊥] Helena Hernandez,[#,▽] Carol V. Robinson,[#,▽] Christopher J. Schofield,*[,⊥] and Inger Andersson*[,||]

Department of Molecular Biology, Swedish University of Agricultural Sciences, Box 590, S-751 24 Uppsala, Sweden, Department of Chemistry, University of Oxford, Chemistry Research Laboratory, Mansfield Road, Oxford OX1 3TA, U.K., and Oxford Centre for Molecular Sciences, Central Chemistry, South Parks Road, Oxford OX1 3QH, U.K.

Received September 22, 2006; Revised Manuscript Received December 1, 2006

ABSTRACT: The ultimate step in the biosynthesis of the medicinally important β-lactamase inhibitor clavulanic acid is catalyzed by clavulanic acid dehydrogenase (CAD). CAD is responsible for the NAPDH-dependent reduction of the unstable intermediate clavulanate-9-aldehyde to yield clavulanic acid. Here, we report biochemical and structural studies on CAD. Biophysical analyses demonstrate that CAD exists as dimeric and tetrameric species in solution. The reaction performed by CAD was shown to be reversible, allowing the use of clavulanic acid for activity analyses. The crystal structure of CAD was solved using single-wavelength anomalous diffraction with a seleno-methionine derivative. The structure reveals that the individual monomers comprise a single domain possessing the Rossmann fold, characteristic of dinucleotide-binding enzymes. The monomers are arranged as tetramers, similar to other tetrameric members of the short-chain dehydrogenase/reductase family. The structure of the unreactive complex of CAD with clavulanic acid and NADPH suggests how CAD is able to catalyze the reduction of clavulanate-9-aldehyde without fragmentation of the bicyclic β-lactam ring structure. The relative positions of NADPH and clavulanic acid, in the active site, together with the presence of the latter in an eclipsed conformation, rationalizes previous labeling studies demonstrating that the incorporation of the C5 *pro-R*, but not *pro-S*, hydrogen of ornithine/arginine into the C9 position of clavulanic acid occurs with overall inversion of configuration.

The discovery of β-lactam antibiotics such as penicillins and cephalosporins represents one of the most important medical breakthroughs, but their continued use is challenged by bacterial resistance. A prevalent mechanism of resistance to β-lactam antibiotics involves hydrolysis of the β-lactam ring catalyzed by β-lactamases. In order to combat this resistance mechanism, two main strategies have been employed: the identification of antibiotics resistant to hydrolysis and the development of β-lactamase inhibitors.

In mechanistic terms, β-lactamases can be divided into two categories, those that employ a metal at the active site and those that utilize a nucleophilic serine. Despite the growing importance of metallo-β-lactamases, serine β-lactamases are the most clinically important. Notably, compounds in clinical use as serine β-lactamase inhibitors are themselves β-lactams. Some possess both antibiotic and β-lactamase inhibitory activities, for example, carbapenems, whereas others are potent β-lactamase inhibitors but lack sufficient antibacterial activity *per se* and are, therefore, administered in combination with more potent antibiotics. The carbapenems are produced by total synthesis, whereas two of the β-lactamase inhibitors in clinical use are synthetic compounds (sulbactam and tazobactam) produced by semisynthesis. However, the most widely used β-lactamase inhibitor is clavulanic acid, isolated from the actinomycete *Streptomyces clavuligerus*. The chemical synthesis of clavulanic acid is hampered by its dense functionality and lability, and therefore, commercial production is achieved by fermentation.

In *S. clavuligerus* the genes for the biosynthesis of both penicillin/cephalosporin β-lactam antibiotics and clavulanic acid are arranged in a super-cluster. Approximately 18 genes (*orf2*−*19*) are proposed to encode for proteins involved in the biosynthesis, transport, and regulation of clavulanic acid (*1*−*3*). The first four enzymes in the biosynthesis pathway have been characterized. N^2-(2-carboxyethyl)arginine synthase (*orf2*) (*4*), β-lactam synthetase (*orf3*) (*5*, *6*), proclavaminate amidinohydrolase (*orf4*) (*7*), and clavaminic acid synthase 2 (*orf5*) (*8*−*11*) are responsible for the conversion of L-arginine and D-glyceraldehyde-3-phosphate into (3*S*, 5*S*)-

[†] This work was supported by grants from the European Union (No. QLK3-CT-2000-00513), the Swedish Natural Science Research Council (VR), and the Biotechnology and Biological Sciences Research Council, U.K.

[‡] Coordinates and structure factors have been deposited at the Protein Data Bank with accession codes 2JAH for the binary complex and 2JAP for the substrate complex.

* To whom correspondence should be addressed. Tel: 44-1865-275625. Fax: 44-1865-275625. E-mail: christopher.schofield@chem.ox.ac.uk (C. J. S.). Tel: 46-18-4714288. Fax: 46-18-536971. E-mail: inger@xray.bmc.uu.se (I. A.).

[§] The contributions of these authors should be considered equal.

[||] Swedish University of Agricultural Sciences.

[⊥] University of Oxford.

[#] Oxford Centre for Molecular Sciences.

[▽] Present address: Department of Chemistry, University of Cambridge, Lensfield Road, Cambridge CB2 1EW, U.K.

10.1021/bi061978x CCC: $37.00
Published on Web 01/19/2007

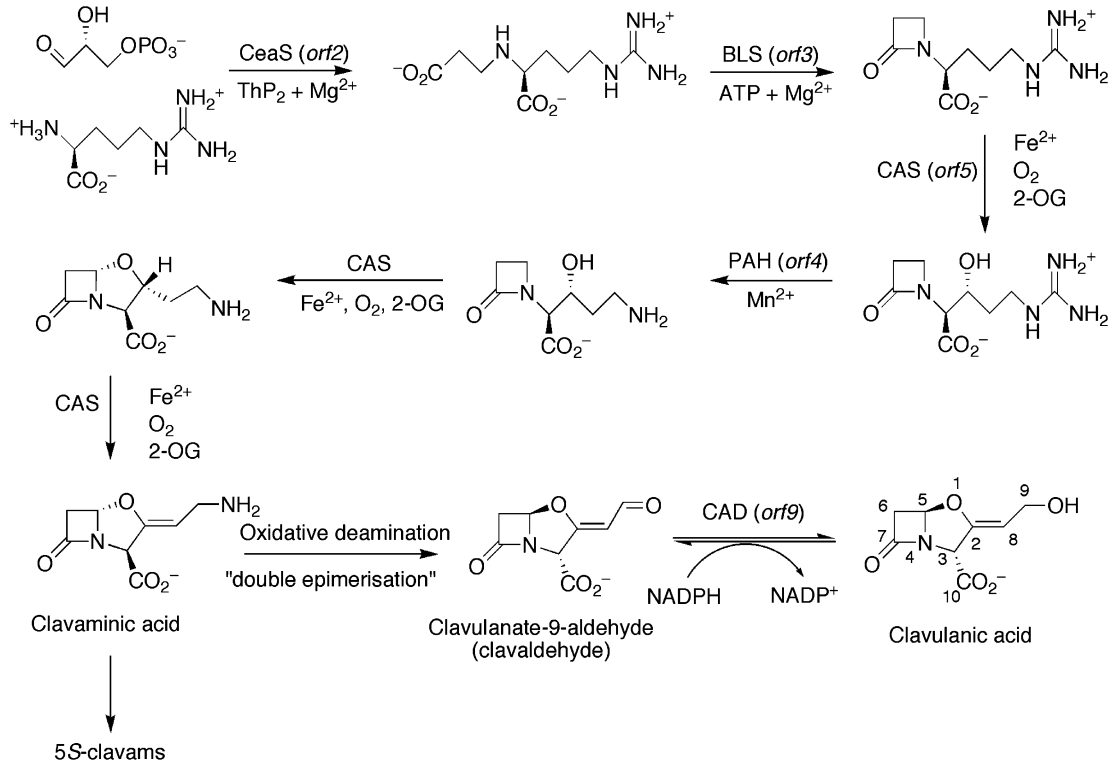

FIGURE 1: Biosynthesis of clavulanic acid. Abbreviations used are N^2-(2-carboxyethyl)arginine synthase, CeaS; β-lactam synthetase, BLS; proclavaminate amidinohydrolase, PAH; and clavaminic acid synthase, CAS.

clavaminic acid (Figure 1). Crystal structures have also been reported for these enzymes (*12*−*15*) as well as for an ornithine acetyltransferase (*orf6*) (*16*) encoded in the clavam gene cluster. Recently, it was shown that *orf17* encodes a *N*-glycyl-clavaminic acid synthetase, catalyzing the addition of glycine to clavaminic acid (*17*). Whether *N*-glycyl-clavaminic acid represents an additional step in the synthesis of clavulanic acid remains unclear at present, as does the function of the remaining ORFs (*orf12*−*19*).

Clavaminic acid serves as a branch point between the biosynthesis of clavulanic acid and other clavams (*18*) that have the 3*S*,5*S* stereochemistry. Clavulanic acid possesses 3*R*,5*R* stereochemistry, like the penicillins, which is required for efficient β-lactamase inhibition. In the remaining steps of clavulanic acid biosynthesis, clavaminic acid must undergo a double epimerization and oxidative deamination to yield (*3R*,*5R*)-clavulanate-9-aldehyde (clavaldehyde), which has been identified as the final intermediate in clavulanic acid biosynthesis (*19*, *20*).

The enzyme encoded by *orf9*, clavulanic acid dehydrogenase (CAD[1]), is responsible for the final step in clavulanic acid biosynthesis. It was first isolated by Nicholson et al. (*19*) and shown to convert clavaldehyde to clavulanic acid in an NADPH dependent reaction (Figure 1). Sequence analysis of CAD revealed homology to enzymes belonging to the short chain dehydrogenase/reductase (SDR) family (*19*). All of the bicyclic intermediates of the clavulanic acid biosynthesis pathway are labile; however, the electron withdrawing properties of the α,β-unsaturated aldehyde renders clavaldehyde especially so, with a half-life of 1 h at neutral pH (*19*, *20*). An important question in clavulanic acid biosynthesis is how such highly labile intermediates are efficiently processed through the pathway. Here, we report the biochemical and crystallographic characterization of CAD. We describe the structure of CAD in complex with NADPH (binary complex) and NADPH and clavulanic acid (ternary complex). The results confirm that CAD is indeed a SDR and suggest how the reduction of clavaldehyde to clavulanic acid is possible without fragmentation of the bicyclic β-lactam ring framework.

MATERIALS AND METHODS

Cloning, Overexpression and Purification for Biochemical Studies. Cad(orf9) was amplified by PCR from the p120KE6.6 plasmid, kindly donated by GlaxoSmithkline PLC, and directly cloned into the PCR-Script vector (Stratagene). The primers used were as follows: forward primer, 5′ − GGT GGT *CAT ATG* CCA TCC GC − 3′; reverse primer, 5′ − GGT GGT *GGA TCC* TCA GAC CTG G − 3′. *Cad* was subsequently cloned into pET24a(+) (Novagen) using NdeI/BamHI restriction sites. The *cad(orf9)*/pET24a(+) construct was transformed into *E. coli* BL21 (DE3) cells. Cells were grown at 37 °C in 2YT media containing kanamycin at 30 μg mL^{-1}. When the cells reached an OD_{600} of 0.5−0.8, the temperature was reduced to 28 °C, and expression was induced by the addition of 1 mM isopropyl thio-β-D-galactoside (IPTG). After a further 4 h, cells were harvested by centrifugation and stored at −80 °C.

A seleno-methionine derivative was prepared by transforming the *cad(orf9)*/pET24a(+) construct into *E. coli* 834 (DE3) cells. Cells were grown at 18 °C to an OD_{600} of 0.6−0.8 in SeMet medium (Molecular Dimensions Ltd, U.K.) using L-seleno-methionine. Upon induction with 0.5 mM

[1] Abbreviations: CAD, clavulanic acid dehydrogenase; NCS, noncrystallographic symmetry; ORF, open reading frame; r.m.s., root-mean-square; SDR, short chain dehydrogenase/reductase.

IPTG, the temperature was raised to 32 °C. Cells were harvested after 6 h and stored at −80 °C.

CAD was purified using a three-step protocol. Cells were resuspended in 50 mM Tris-HCl (pH 7.5) and lysed by sonication. The lysate was cleared by centrifugation, and the supernatant was loaded onto a Q-sepharose column and eluted with a NaCl gradient. The peak fractions were pooled and loaded onto a Phenyl-Resource column in 50 mM Tris-HCl (pH 7.5) and 1 M $(NH_4)_2SO_4$. Protein was eluted using a reverse $(NH_4)_2SO_4$ gradient. Size exclusion chromatography (Superdex S200) was used as a final step to yield CAD of >90% purity by SDS−PAGE analysis. The purified protein was desalted and stored at −80 °C in 10 mM Tris-HCl (pH 7.5).

Purification of the seleno-methionine derivative was performed as described above with β-mercaptoethanol (5 mM) present in all buffers. The purified CAD protein was stored in 5 mM HEPES (pH 7.5), 1 mM EDTA, and 5 mM β-mercaptoethanol.

Crystallization. Crystallization experiments were performed using the hanging-drop vapor diffusion method. The addition of 2 mM NADPH to the protein solution was necessary to obtain sufficiently ordered crystals. Crystals were initially obtained under several different conditions in Clear Screen I (Molecular Biosciences Ltd., U.K.) with cacodylate as the buffering agent. In order to avoid contaminating anomalous signals from cacodylate at wavelengths close to the selenium absorption edge, Bis-Tris was used as a buffering agent for the crystallization of the seleno-methionine derivative. Diffracting crystals of the seleno-methionine derivative were obtained by seeding from small crystals into a drop consisting of 2 μL of protein (ca. 3 mg/mL in 5 mM HEPES (pH 7.5), 1 mM EDTA, 5 mM β-mercaptoethanol, and 2 mM NADPH) and 2 μL of reservoir solution consisting of 10% PEG 1000, 10% PEG 8000, 0.3 M sodium acetate, and 0.05 M Bis-Tris buffer (pH 6.5). After 1 to 3 days at 22 °C, crystals grew to approximately 100 × 40 × 40 μm^3. For data collection at cryogenic temperatures, crystals were transferred to a cryo-solution consisting of the reservoir solution containing 25% PEG 400, followed by submersion in liquid nitrogen. Crystals of the native protein used for substrate soaks were obtained by mixing equal volumes of protein (ca. 5 mg/mL in 5 mM HEPES (pH 7.5), 1 mM EDTA, 5 mM β-mercaptoethanol, and 2 mM NADPH) and a reservoir solution containing 25% PEG 2000 monomethyl ether, 0.8 M sodium formate, and 0.1 M cacodylate buffer (pH 6.5). Crystals were transferred to a mother liquor solution containing 10 mM clavulanic acid and cryo-protectant for 10 min prior to flash-freezing in liquid nitrogen.

Data Collection and Structure Determination. Single-wavelength anomalous diffraction (SAD) data to 1.8 Å were collected from a crystal of seleno-methionine derivatized enzyme at ID14-3 (ESRF, Grenoble, France) at 100 K on a MAR CCD detector (Table 1). The data were processed using DENZO/SCALEPACK (*21*), MOSFLM (*22*, *23*), and SCALA (*22*). The crystals belong to space group $P2_12_12_1$, with unit cell dimensions $a = 58$ Å, $b = 122$ Å, and $c = 126$ Å (Table 1). Assuming the presence of four molecules in the asymmetric unit gave a V_M of 2.2 $Å^3$ Da^{-1} (*24*) with 42.7% solvent. A self Patterson (*22*) revealed the presence of a noncrystallographic symmetry (NCS) translation peak.

Table 1: Statistics for Data Collection and Phasing

	SeMet derivative (binary complex)	substrate complex (ternary complex)
X-ray source	ID14:3 (ESRF)	BM14 (ESRF)
wavelength (Å)	0.934	0.979
space group	$P2_12_12_1$	$P2_12_12_1$
cell dimensions *a*, *b*, *c* (Å)	58.7, 122.6, 126.6	58.1, 123.4, 126.8
resolution range (Å)	29.9−1.8 (1.9−1.8)[a]	34.9−2.1 (2.2−2.1)
no. of measurements	417,910 (39,798)	264,726 (34,519)
no. of unique reflections	82,024 (9,815)	53,663 (7,610)
completeness	96.2 (80.6)	99.4 (98.3)
anomalous completeness	92.5 (68.4)	
mean $I/\sigma(I)$	19.1 (3.7)	14.6 (3.4)
multiplicity	5.1 (4.1)/2.7 (2.3)[c]	4.9 (4.5)
R_{meas}[b]	0.069 (0.389)	0.093 (0.397)
no. of Se sites	24	
figure of merit (centric/acentric)	0.1348/0.345	
phasing power	1.105 (0.33)	

[a] Values in parentheses indicate the outer resolution shell. [b] R_{meas} is as defined by Diederichs and Karplus (*60*). [c] The second set refers to anomalous data.

The selenium sites were located using the SHELX suite (*25*), and the sites were refined using AUTO-SHARP (*26*). After solvent flattening and density modification in SOLOMON (*27*), the use of ARP-wARP (*28*) (implemented in AUTO-SHARP) resulted in tracing of ca. 50% of the main-chain residues in the tetramer. Using the model of a related SDR from *Mycobacterium tuberculosis*, Rv2002 (pdb code 1NFF (*29*)), a mask was prepared and the NCS operators determined, allowing electron density averaging using the RAVE suite of programs (*30*). Further model building was performed by additional ARP-wARP cycles and by the manual building of residues into the averaged maps using O (*31*).

The model was initially refined in CNS (*32*) using simulated annealing with 4-fold NCS constraints and unbiased HL coefficients from auto-SHARP. Difference maps clearly showed the presence of the cofactor, NADPH. Although the puckering of the nicotinamide ring associated with the reduced state of the cofactor was not discernible in the maps, parameters for the reduced cofactor were used during refinement. Refinement was continued with a gradual relaxation of the NCS restraints. The final stages of refinement were performed in REFMAC5 (*33*) using TLS refinement (*34*) with each monomer as a TLS group. Solvent molecules were added using ARP-wARP (*35*) and were manually inspected in O (*31*). The final model has an R_{factor} of 18.2% and an R_{free} value of 20.9% (Table 2).

Data for the substrate complex were collected on BM14 (ESRF, Grenoble, France) at 100 K on a MAR CCD detector (Table 1). Diffraction images were processed using MOSFLM (*22*, *23*) and SCALA (*22*). The unit cell dimensions were isomorphous to those of the seleno-methionine derivative; therefore, a model was obtained by rigid body refinement followed by simulated annealing in CNS, using 4-fold NCS constraints. Difference maps clearly showed the presence of NADPH and clavulanic acid; the latter was omitted for several rounds of refinement. The structure of clavulanic acid was obtained from the Cambridge Structural Database (*36*) and a torsion restraints library prepared using XPLO2D (*37*) for use in O (*31*). Refinement continued using TLS refinement with REFMAC5 and resulted in a final model of

Table 2: Refinement Statistics

	binary complex	ternary complex
R_{cryst}[a]	18.2%	18.4%
R_{free}[b]	20.9%	21.6%
Wilson *B* factor (Å^2)	19.3	28.5
rmsd from ideal geometry		
bond lengths (Å)	0.010	0.009
bond angles (°)	1.295	1.562
Ramachandran outliers[c]	1.3%	1.3%
no. atoms/average *B* factor		
molecule A	1840/21.8	1832/32.8
molecule B	1840/32.5	1832/44.8
molecule C	1858/23.6	1850/33.8
molecule D	1832/30.9	1832/41.1
NADPH A-mol	48/21.3	48/30.6
NADPH B-mol	48/29.6	48/41.7
NADPH C-mol	48/20.2	48/30.8
NADPH D-mol	48/30.1	48/40.6
clavulanic acid A-mol		14/33.1
clavulanic acid B-mol		14/39.9
clavulanic acid C-mol		14/37.4
clavulanic acid D-mol		14/38.8
solvent	494/27.4	254/31.6

[a] $R_{cryst} = \Sigma_{hkl}||F_o|-|F_c||/\Sigma_{hkl}|F_o|$ where F_o and F_c are the observed and calculated structure factor amplitudes, respectively. [b] R_{free} is calculated from a randomly chosen 5% sample of all unique reflections. [c] These are defined according to Kleywegt and Jones (*61*).

the substrate complex with an $R_{factor} = 18.4\%$ and $R_{free} = 21.6\%$. Solvent-accessible buried surface calculations were performed using CNS (*32*). Figures 4−8 were prepared using PyMOL (*38*).

CAD Activity Assays. CAD was assayed for activity by UV spectrophotometry at 25 °C, measuring the production of NADPH at 340 nm using a molar extinction coefficient for NADPH of 6.22 mM^{-1} cm^{-1}. The reaction mixture consisted of a 1 mL solution of 100 mM Bis-Tris-HCl (pH 6.5), 1−8 mM $NADP^+$, and 0.5−8 mM clavulanic acid. The reaction was initiated by the addition of 2 μg of enzyme. In order to determine the pH profile, reactions were performed as above, with the concentration of $NADP^+$ and clavulanic acid kept at 5 mM, in 100 mM buffer, covering the pH range 6−9. The buffers used were: Bis-Tris-HCl at pH 6.0−7.5 and Tris-HCl at pH 7.5−9.0.

For ^{1}H NMR (500 MHz) assays, the reagents were made up in D_2O prior to mixing in the NMR tube to final concentrations of 100 mM Bis-Tris-HCl (pH 6.5), 20 mM $NADP^+$, and 20 mM clavulanic acid. The ^{1}H NMR (500 MHz) spectrum was recorded immediately after the addition of 20 μg of enzyme.

Molecular Weight Determination (by Gel Filtration). The native molecular weight of CAD was determined by size exclusion chromatography (Superdex 200 HR) using cytochrome c (12 kDa), chymotrypsin (25 kDa), ovalbumin (43 kDa), bovine serum albumin (67 kDa), aldolase (158 kDa), and blue dextran (2000 kDa) (GE Healthcare Life Sciences) as calibration standards.

Mass Spectrometric Studies of Native CAD. The sample was supplied at 7 mg/mL (266 μM monomer) concentration. An aliquot of CAD (8 μL) was diluted to 30 μL with 100 mM ammonium acetate (pH 7.0) and desalted twice using Biospin-6 microcentrifuge columns prior to use. The final concentration was 26 μM monomer. Data were acquired using a modified QToF2 mass spectrometer (*39*) (Waters, Manchester, U.K.) configured for nanoflow ESI in positive ion mode. The tetramer was observed using collisional cooling (through throttling the rotary pump isolation valve) to give instrument pressures of 3.2×10^{-3} mbar source, 2.4×10^{-5} mbar analyzer, and 5.4×10^{-7} mbar ToF. Source conditions were as follows: capillary, 1.8 kV; cone, 200 V; and extractor 0 V.

RESULTS AND DISCUSSION

Expression, Purification, and Characterization of Recombinant CAD. Previous studies on CAD have been performed on the native enzyme purified from *S. clavuligerus* by a procedure using red-sepharose resin (*19*). In order to obtain sufficient quantities of CAD for biochemical and structural studies, the *cad* gene was cloned and the recombinant protein overexpressed in *E. coli*. The resultant protein was purified to near homogeneity in a three-step protocol. The enzyme migrated as a protein of approximately 27 kDa by SDS−PAGE analysis and gave a mass of 26192 Da by ESI mass spectrometry, close to the predicted mass of CAD minus the N-terminal methionine (26194 Da). Edman sequencing of the recombinant CAD confirmed an N-terminal sequence of PSALQGKVAL, consistent with the observations of Fulston et al. (*20*) and contrary to previous studies with wild-type CAD, suggesting that the second amino acid (Pro[2]) was also absent[2] (*19*, *40*).

Native gel electrophoresis indicated that CAD exists as a tetramer in solution and that the presence of the substrate and/or cofactor did not affect the oligomeric state. During gel filtration chromatography, CAD eluted as an asymmetric peak, corresponding to both a dimeric and tetrameric form, suggesting that these two states may be in equilibrium. Further investigation using mass spectrometry (Figure 2) indicated that the major species observed corresponds to a tetramer (calculated mass: 104776 Da). Dimeric, monomeric, and a low level of octameric species were also observed in the mass spectra. The tetramer was found to be stable over the range of conditions used, with no significant increase in the relative intensities of dimeric and monomeric species.

Enzymatic Activity Analyses. CAD is responsible for the reduction of clavaldehyde to clavulanic acid, using NADPH as a cofactor. With a half-life of approximately 1 h (*19*), the preparation and storage of clavaldehyde is difficult and analysis of the reaction complicated. However, NAD(P)H dependent SDRs often catalyze reversible reactions. We were able to observe the oxidation of clavulanic acid to clavaldehyde by CAD in the presence of $NADP^+$, which is contrary to previous attempts to oxidize clavulanic acid (*20*).

Clavaldehyde has an absorption maximum at 262 nm due to the allylic aldehyde chromophore. However, because of the strong absorption at 260 nm by the nicotinamide ring of the oxidized cofactor, it was not possible to directly follow the production of the aldehyde. Instead, the reaction could be monitored by UV spectroscopy at 340 nm because of the additional absorption peak of the reduced cofactor nicotinamide ring. In the presence of CAD and clavulanic acid, $NADP^+$ was reduced to NADPH. Experiments verified the observation of Fulston et al. (*20*) that NADH cannot

[2] The X-ray diffraction studies revealed electron density for Pro[2] only in the "C molecule" in both binary and ternary complex structures, suggesting that Pro[2] is quite motile, although the possibility of N-terminal degradation cannot be excluded.

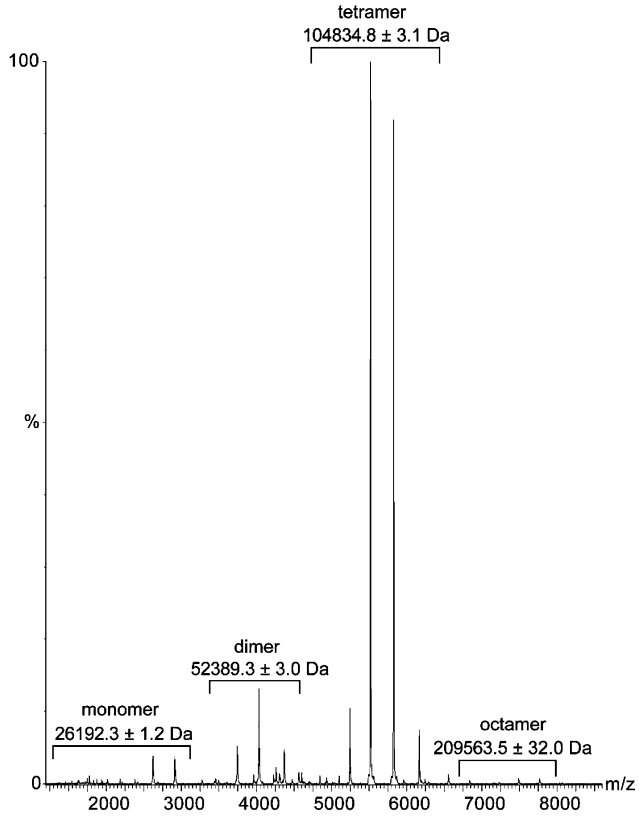

FIGURE 2: Nanoflow electrospray ionization mass spectrum of CAD showing the different oligomeric forms observed.

substitute for NADPH as a cofactor. The pH profile of CAD was determined by the UV assay, and maximal enzyme activity was observed between pH 6.5 and 7.0.

^{1}H NMR spectroscopy was used to confirm that the reverse reaction product was indeed clavaldehyde and that NADPH production was not due to uncoupled turnover. Spectra (Figure 3) of the crude reaction mixture were obtained for the reverse reaction in D_2O. Because of the reactivity and instability of clavaldehyde, the reaction was not quenched but instead the reagents prepared in D_2O and the reaction carried out in an NMR tube. Time-course experiments enabled the observation of a doublet at 9.7 ppm, assigned as the aldehyde proton of clavaldehyde. A new doublet peak at 5.5 ppm corresponding to the vinylic hydrogen was also visible. These values are consistent with literature NMR assignments for clavaldehyde (*20*). To validate the assumption that these two new peaks both resulted from the production of an α,β-unsaturated aldehyde, a homonuclear decoupling experiment was performed. Irradiation of the doublet at 9.7 ppm resulted in a collapse of the doublet at 5.5 ppm to a singlet, confirming that these protons are indeed coupled. (Figure 3). A 2D ^{1}H NMR spectrum also supported the assignment of the product as clavaldehyde.

A noticeable increase in product concentration was observed between spectra taken at $T = 5$ min and $T = 1$ h, but beyond this time, no product formation was apparent. Further addition of enzyme at this point did result in additional product formation, but the maximum turnover observed at this point was approximately 5% of the total. Fulston et al. (*20*) reported that the reduction of clavaldehyde to clavulanic acid in the presence of NADPH was complete on mixing of the reagents. Together, the results indicate that the equilibrium of the reaction mixture probably lies on the side of clavulanic acid and $NADP^+$ and is consistent with the low levels of clavaldehyde produced in the NMR assay. Overnight incubation resulted in a reduction of the intensity of the product peak and the appearance of additional peaks in the NMR spectra. This observation is consistent with the instability of clavaldehyde leading to degradation in solution over longer times.

Sequence and Structural Analysis of CAD. Sequence analysis of CAD reveals homology to enzymes belonging to the SDR family (*19*), which is consistent with the fact that NADPH was essential for obtaining suitable diffracting crystals. Approximately 3000 SDR family members have been identified, with wide ranging and diverse substrate specificities, including alcohols, sugars, steroids, and aromatic compounds. Only a small number of highly conserved residues characterize the SDR family, which otherwise shows relatively low sequence identity, in the order of 15−30%. Despite this, the 3D structures of the SDRs show a similar fold (*41*). The structural studies revealed that CAD consists of a single domain subunit, possessing the characteristic Rossmann fold (*41*) (Figure 4) common to dinucleotide-binding enzymes. The core of the enzyme is formed by seven β-strands (βA−βG) creating a parallel β-sheet, which is in turn surrounded by eight α-helices (αB−αG). The β-sheet is flanked on one side by helices αC, αB, and αG and on the other side by helices αD, αE, and αF. Helix αFG1 lies above the β-sheet, with its helical axis pointing toward the pyrophosphate moiety of the nucleotide cofactor NADPH, whereas helix αFG2 lies on the top edge of the β-sheet and helps to form a protective lid over the active site.

The crystallographic data confirmed the solution and mass spectrometric studies on the oligomeric state of CAD. The four molecules within the asymmetric unit are arranged as a tetramer (Figure 5), similar to the structures of other tetrameric SDRs. The CAD monomers are arranged with 222 symmetry generating three 2-fold axes, labeled *P*, *Q*, and *R* following the assignment of Rossmann (*42*). The interface around the *P* axis (A and B monomers) has a solvent-accessible buried surface of 1390 Å^2 per monomer (ca. 13%) and is formed through both hydrogen-bonding and hydrophobic interactions involving helix αG and the extension of β-strand βG. The *Q* interface (monomers A and C) is formed by the hydrophobic interactions of helices αE and αF from each monomer, forming a four-helix bundle with an average surface interaction area of 1631 Å^2 per monomer (ca. 16%). Interactions along the *R* axis (monomers A and D) contribute little to the tetramer interactions, with an average surface interaction area of only 80 Å^2 per monomer. This is considerably less than that observed in tetrameric SDRs from other species, for example, 3α,20β-hydroxysteroid dehydrogenase (*43*), β-acyl carrier protein reductase (*44*), *meso*-2,3-butanediol dehydrogenase (*45*), or Rv2002 (*29*), and is due to the short C-terminus of CAD (Figure 6).

In addition to the differences observed in the C-terminal region, the largest variation in the SDR structures are found in the region around helices αFG1 and αFG2, which form part of the substrate binding site (*46*, *47*). Despite low sequence homology among SDR family members, motifs that define classical SDRs are apparent. A conserved Asn^{90}-Asn^{91}-Ala^{92}-Gly^{93} sequence is important for the stabilization of the central β-sheet (*48*), as is the conserved glycine rich Thr^{13}-

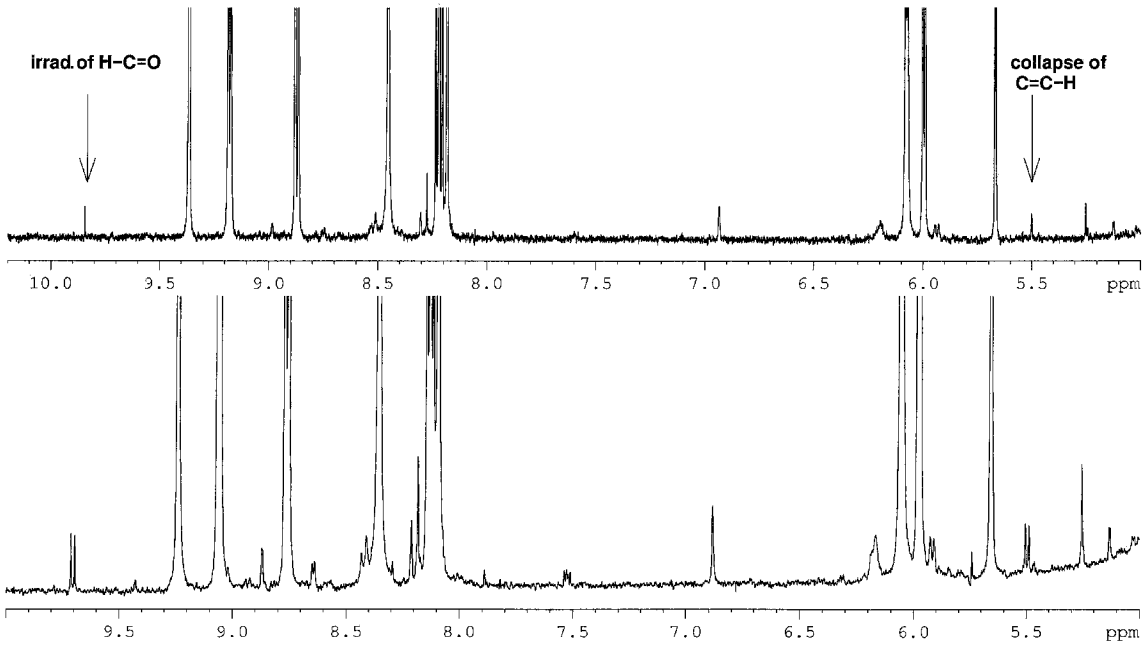

FIGURE 3: Homonuclear decoupling ^{1}H NMR spectrum of the CAD-catalyzed reaction showing the collapse of the doublet corresponding to the vinylic proton (5.5 ppm) upon irradiation of the adjacent aldehyde proton (9.7 ppm).

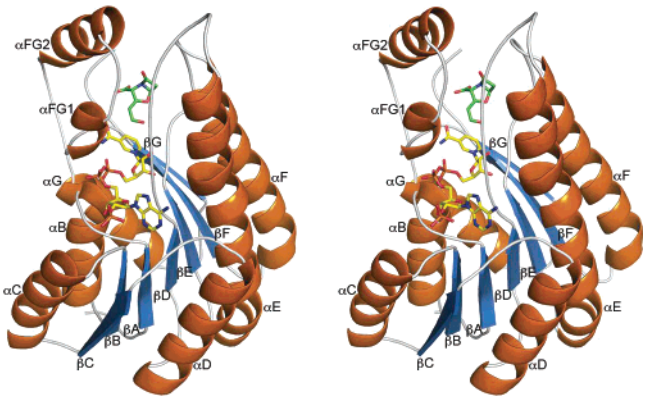

FIGURE 4: Secondary structure of CAD. The parallel β-sheet consisting of seven β-strands (blue) is surrounded by eight α-helices (orange) with loops shown in gray. The NADPH cosubstrate (yellow) and clavulanic acid (green) are shown as sticks.

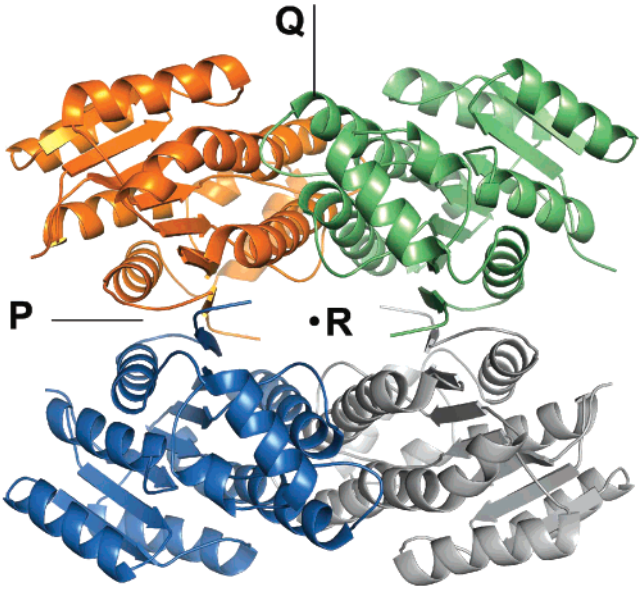

FIGURE 5: Tetrameric arrangement of molecules A (orange), B (blue), C (green), and D (gray) in the asymmetric unit of the crystal. The *P*, *Q*, and *R* axes (*41*) are indicated, where axis *R* is parallel to the point of view, i.e., perpendicular to the plane of the page.

Gly^{14}-X$_3$-Gly^{18}-X-Gly^{20} motif, which is involved in the binding of the dinucleotide cofactor (*49*). The residues forming the catalytic triad (Ser^{142}, Tyr^{155}, and Lys^{159}), which define reductase activity (*49*), have been extended to include Asn^{115} (*48*, *50*), which is also conserved in CAD. The conserved water molecule associated with Asn^{115} is also present (e.g., water Z25 in the A molecule of the ternary complex) and may have functional importance (see below). Another conserved water is linking the glycine rich nucleotide binding motif to the dinucleotide pyrophosphate and the C-terminal residue (Asn^{91}) of βD (*51*) (e.g., water Z50 in the A molecule of the binary complex).

Cofactor Binding. The absolute dependence of CAD on NADP(H) in favor of NAD(H) demonstrated here and earlier by Fulston et al. (*20*) is consistent with its structure. Classical SDRs that bind NAD(H) have an acidic residue at the end of strand βB, where as in CAD, this position is occupied by the nonpolar residue Ala^{38}. NADP(H) binding enzymes typically possess two characteristic basic residues: the first immediately preceding the second glycine of the cofactor-binding motif and the second positioned directly after the crucial acidic residue of NAD(H)-preferring enzymes (*47*, *52*). In CAD, this corresponds to residues Ser^{17} and Arg^{39} and demonstrates that the requirements for basic residues are not absolute. Thus, CAD can be classified as belonging to the cP2 subfamily as defined by Kallberg et al. (*52*).

NADPH was clearly observed in the electron density of both the binary and ternary CAD complex structures. The cofactor is bound in an extended conformation in the binding pocket (Figure 7). The degree of extension in other SDRs has been measured by using the distance between the C6 carbon of the adenine ring and the C2 carbon of the nicotinamide group of NADPH in the syn conformation (*53*). In CAD, this distance is 13.8 Å, which is similar to that of

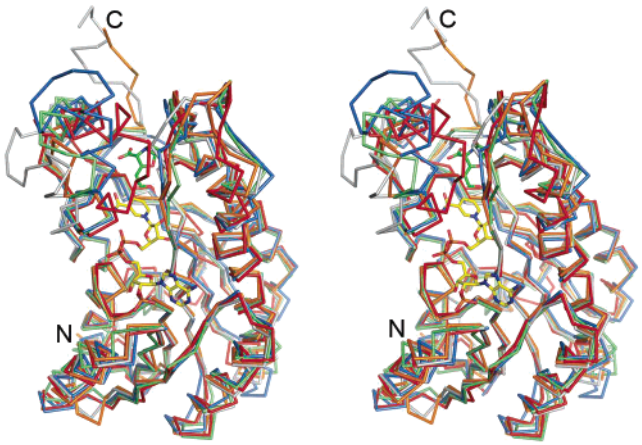

FIGURE 6: Conservation of tertiary structure in CAD and selected SDR enzymes. The SDRs represented (color and pdb code) are CAD (red, 2JAP), 3α,20*β*-hydroxysteroid dehydrogenase (gray 2HSD (*43*)) *β*-keto acyl carrier protein reductase, (green, 1EDO (*44*)), *meso*-2,3-butanediol dehydrogenase (blue, 1GEG (*45*)), and Rv2002 (orange, 1NFF (*29*)). The cofactor NADPH (yellow) and clavulanic acid (green) are depicted as sticks. Rms deviation on Cα atoms, calculated using O (*31*) and sequence identities (SI) to CAD, are as follows. 2HSD: rmsd = 1.213 Å for 207 atoms; SI = 33%. 1EDO: rmsd = 1.267 Å for 217 atoms; SI = 28%. 1GEG: rmsd = 1.246 Å for 215 atoms; SI = 31%. 1NFF: rmsd = 1.316 Å for 212 atoms; SI = 38%.

other SDRs. The cofactor binding pocket has a solvent-accessible buried surface of ca. 1325 Å^2 and is located at the C-terminal end of the central *β*-sheet (comprising strands *β*B, *β*A, *β*D, and *β*E) (Figures 3 and 7). Strands *β*C and *β*F form two sides of the cofactor binding pocket, binding the adenine and nicotinamide moieties, respectively. The adenine binding pocket is lined with hydrophobic residues (Gly^{14}, Ala^{38}, Val^{65}, Ala^{92}, and Ile^{94}) and is isolated from the external solvent by Arg^{39}. A hydrophobic floor in the nicotinamide ring-binding pocket is created by residues Ile^{19}, Met^{140}, Pro^{185}, and Thr^{188}, whereas polar residues on the opposite side direct and facilitate substrate binding and catalysis of the aldehyde reduction. Lys^{159} forms bifurcated hydrogen bonds to both 2′ and 3′ hydroxyl groups of the cofactor nicotinamide ribose, coordinating the cofactor as well as helping to lower the p*K*a of the catalytic base Tyr^{155} (*54*) (see below). The glycine rich nucleotide binding motif (see above) in the loop between *β*A to αB interacts with the pyrophosphate moiety of NADPH, forming hydrogen bonds to the phosphate oxygens. The dipole charge of helix αB may assist in the stabilization of the pyrophosphate group, and likewise, helix αFG1 may stabilize in a similar way, albeit to a lesser degree.

Substrate Binding and Reaction Mechanism. In *S. clavuligerus*, CAD catalyzes the reduction of clavaldehyde to clavulanic acid. Because of the inherent instability of the α,*β*-unsaturated aldehyde of clavaldehyde, a crystal complex was instead prepared using clavulanic acid. The cocrystallization of CAD and NADPH and the subsequent soaking of clavulanic acid into the crystal ensured that a nonproductive complex was formed, that is, clavulanic acid cannot be oxidized to clavaldehyde in the presence of NADPH.

Unlike some of the other SDR enzymes, for example, 7α-hydroxysteroid dehydrogenase reductase (*55*), crystalline CAD does not appear to undergo a significant conformational change upon binding of the substrate. Alignment of the binary NADPH complex and the ternary substrate complex reveals that there is no significant movement within the subunit upon binding of the substrate (rms deviation 0.189 Å for 981 Cα atoms). Indeed, the only residue within the substrate-binding site to change conformation is Arg^{208}. The Arg^{208} side chain appears to be quite motile in both the binary and ternary complex structures, with average RSCC values (*31*) of 0.823 and 0.877, respectively. In the binary complex with NADPH, the side chain of Arg^{208} lies predominantly to one side, leaving a small tunnel open to the substrate. Upon substrate binding, Arg^{208} moves to a position so as to lie directly over the binding pocket (Figure 8), closing the entrance to the binding site to the external solvent. Arg^{208} also interacts with the C3 carboxyl moiety through solvent-mediated hydrogen bonding.

The solvent-accessible buried surface of the substrate-binding cleft is ca. 480 Å^2 and is located on the periphery of the molecule between helices αFG1 and αFG2 (Figure 3). The residues that form the catalytic triad/tetrad are located toward the hydrophobic core of the protein in the loop between *β*E and αF (Ser^{142}) and in helix αF (Tyr^{155} and Lys^{159}). This results in the reactive *C*9-aldehyde of the substrate being sequestered away from the aqueous environment of the surface, preventing adventitious hydrolysis. Several hydrogen bonds are responsible for coordinating the binding of clavulanic acid within the active site (Figure 8). Ser^{142} forms a hydrogen bond to the *C*9-hydroxyl of clavulanic acid, which is further stabilized by the additional

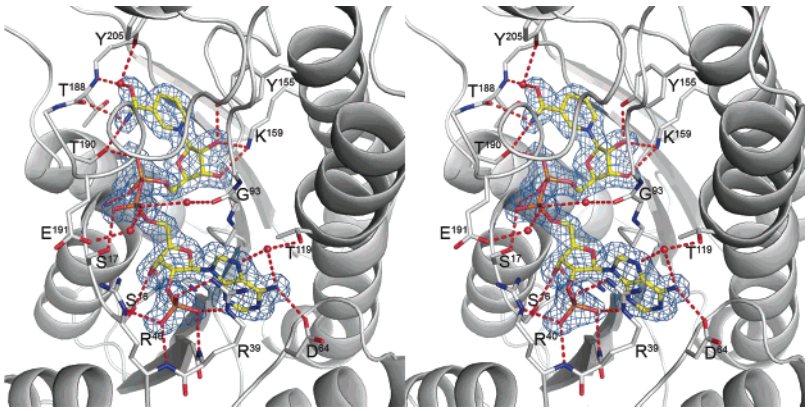

FIGURE 7: Cofactor binding in CAD. Proposed hydrogen bond interactions between the protein (gray) and NADPH (yellow) are shown as red dashes. Water molecules are depicted as red spheres. The $2mF_{obs} - DF_{calc}$ electron density at the NADPH molecule is contoured at 1σ and is shown in blue. Helix αFG1 has been represented as a loop for clarity.

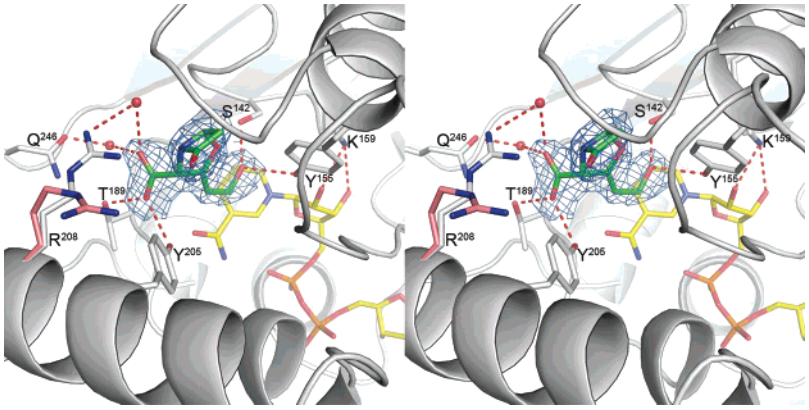

FIGURE 8: Binding of clavulanic acid in the active site and the movement of Arg^{208} upon substrate binding. Proposed hydrogen bonding interactions between the protein (gray) and clavulanic acid (green) are shown as red dashes. The bifurcated hydrogen bond formed between Lys^{159} and the ribose oxygens of NADPH (yellow) is also shown. The conformation of Arg^{208} from the binary complex is shown (salmon) pointing away from the active site. Water molecules are depicted as red spheres. The $2mF_{obs} - DF_{calc}$ electron density for the clavulanic acid molecule is contoured at 1σ and is shown in blue. Note the lack of hydrogen bonding to the β-lactam carbonyl.

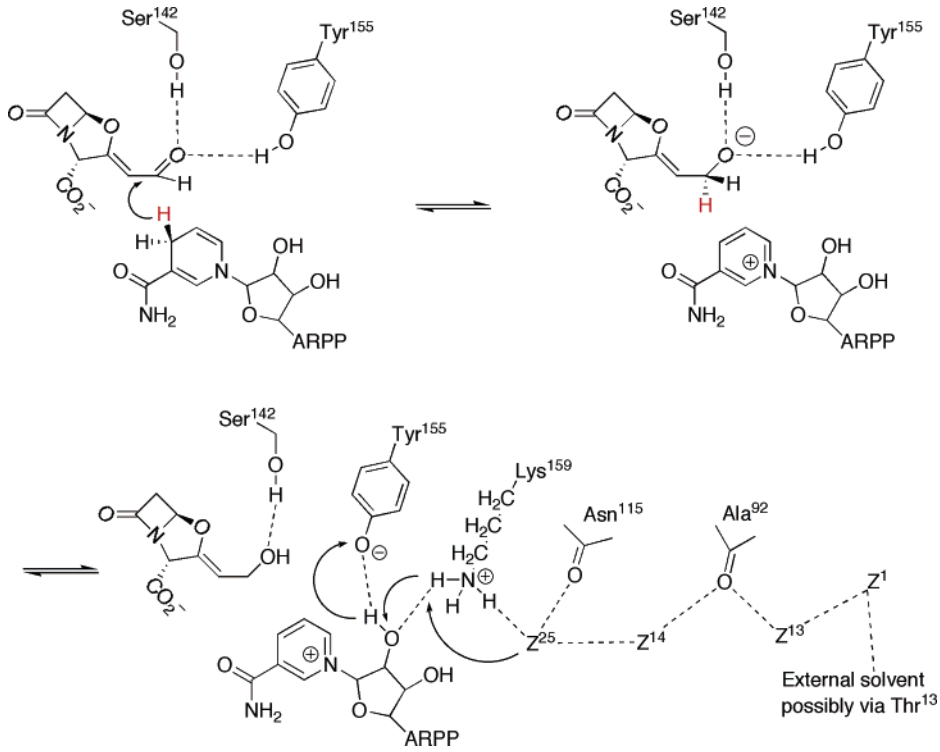

FIGURE 9: Proposed reaction mechanism for the CAD catalyzed reaction and possible proton relay. The numbering of waters refers to the water molecules in the A molecule of the ternary complex. ARPP is the adenosine ribose pyrophosphate moiety of NADP(H). For the numbering of clavaldehyde/clavulanic acid, see Figure 1.

interaction of the *C*9-hydroxyl with the catalytic base Tyr^{155}. This positions the C9 carbon of clavulanic acid ca. 2.5 Å above the *pro-S* hydrogen of the nicotinamide ring, with an angle of 123° formed between the C4 hydrogen of NADPH and carbon C9 of clavulanic acid. Additional coordination of clavulanic acid in the binding pocket is achieved by the hydrogen bonding of the C3 carboxyl moiety to Thr^{187} and Tyr^{205} as well as via solvent interactions to Gln^{246} and Arg^{208} (e.g., Z58 and Z68 in the A molecule of the ternary complex). It is interesting to note that the β-lactam C7 carbonyl points toward a hydrophobic pocket and does not participate in hydrogen bonding. A similar situation is observed in the binding of the monocyclic clavulanic acid biosynthesis intermediate proclavaminic acid to clavaminic acid synthase (CAS) (pdb code 1DRT (*14*)). In the case of β-lactam synthetase (BLS), the β-lactam carbonyl of deoxyguanidinoproclavaminic acid does form a hydrogen bond to Lys^{443} (pdb code 1MC1 (*56*)). However, BLS differs from CAS and CAD in that it actually catalyzes formation of the β-lactam ring via an ATP activated β-amino acid. It is possible that hydrogen bonding to the β-lactam carbonyl groups of either clavaminic acid (CAS) or clavaldehyde (CAD) would facilitate hydrolysis and is consequentlyavoided in substrate binding. Indeed, the mechanism by which clavulanic acid inhibits β-lactamases involves β-lactam ring opening mediated by a nucleophilic serine residue attacking the C7 carbonyl.

The position of clavulanic acid and NADPH within the active site is consistent with the common proposed mechanism for SDR oxidoreductases (*47*, *49*) in which the 4-*pro-S* hydrogen of NADPH is transferred to the carbonyl group of the substrate (Figure 9). The hydrogen bonding of the *C*9-

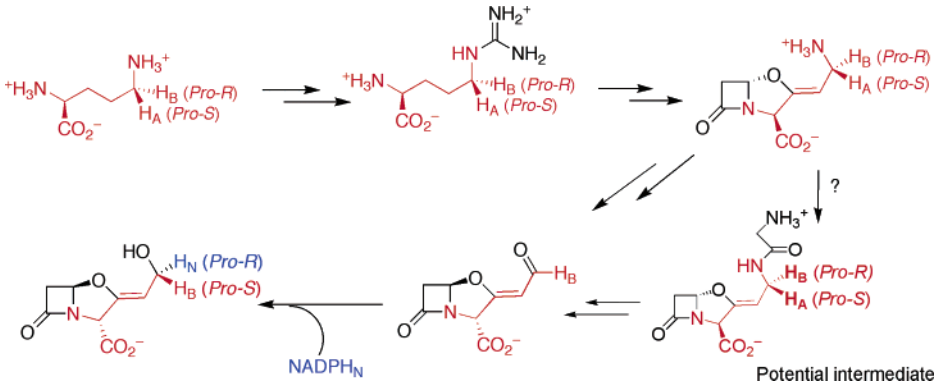

FIGURE 10: Overview of labeling studies (*59*) showing the origin of the C9 hydrogens of clavulanic acid with respect to its precursor ornithine/arginine. Also shown is a potential glycyl-clavaminic acid acid intermediate (*17*).

aldehyde to Ser[142] and Tyr[155] probably promotes nucleophilic attack by the hydride. The resulting positive charge on the oxidized nicotinamide ring may help reduce the p*K*a of Tyr[155], allowing proton transfer from the tyrosine hydroxyl group to the alkoxide formed during the reduction step. Subsequently, Tyr[155] could be re-protonated via a proton relay system, where protons are extracted and transferred from surrounding water molecules located in a small hydrophilic pocket (*48*, *50*). This is likely to occur after $NADP^+$ has been displaced from the active site and is replaced by NADPH. Residues Thr[13], Asn[90], Ala[92], Thr[114], and Asn[115] may play a role in stabilizing the water molecules to allow proton transfer in an otherwise hydrophobic environment. The proton relay proposed for CAD is similar to that proposed for the 3β/17β-hydroxysteroid dehydrogenase (*48*), with the exception of Ser[114] in the 3β/17β-hydroxysteroid dehydrogenase because the corresponding residue in CAD is a glycine residue (Gly[118]).

The observed conformation of clavulanic acid is such that the C9−OH bond adopts an eclipsed conformation in which it projects toward the clavam oxygen and is almost coplanar with the O1−C2 and exocyclic alkene bonds (Figure 9). This conformation contrasts with that observed in small molecule crystal structures of clavulanate (*57*, *58*) in which the C9−OH bond points away from the clavam ring nucleus (e.g., as shown for clavulanic acid in Figure 1). The observed eclipsed conformation in the active site enables hydride transfer to occur to the *re*-face of the aldehyde, resulting in the transferred hydrogen occupying the *pro-R* methylene position of clavulanic acid.

The proposed stereochemical course of the CAD-catalyzed clavaldehyde reduction rationalizes labeling studies on the origin of the hydrogens at the C9 position of clavulanic acid. Work using ornithine (a precursor of arginine, which is required for the first committed step of the pathway) labeled at its *pro-R* and *pro-S* positions demonstrated that the *pro-R*, but not the *pro-S* hydrogen, was incorporated at the C9 position of clavulanic acid (*59*). Furthermore, these studies demonstrated that the incorporation of the ornithine C5 *pro-R* hydrogen occurs with overall inversion such that it is observed at the C9 *pro-S* position of clavulanic acid and thus implies that the C5 *pro-S* hydrogen of ornithine/arginine must be lost from glycyl-clavaminic/clavaminic acid in the formation of clavaldehyde (Figure 10). The addition of the hydride ion to the *re*-face of the observed eclipsed conformation in the CAD active site rationalizes the overall inversion of the configuration from the C5 position of ornithine to the C9 position of clavulanic acid.

ACKNOWLEDGMENT

We thank the staff of the ESRF (Grenoble, France) for outstanding support at the synchrotron. We are indebted to Barbara O'Dell for assistance with NMR measurements.

REFERENCES

1. Hodgson, J. E., Fosberry, A. P., Rawlinson, N. S., Ross, H. N., Neal, R. J., Arnell, J. C., Earl, A. J., and Lawlor, E. J. (1995) Clavulanic acid biosynthesis in *Streptomyces clavuligerus*: gene cloning and characterization, *Gene 166*, 49−55.
2. Li, R., Khaleeli, N., and Townsend, C. A. (2000) Expansion of the clavulanic acid gene cluster: identification and in vivo functional analysis of three new genes required for biosynthesis of clavulanic acid by *Streptomyces clavuligerus*, *J. Bacteriol. 182*, 4087−4095.
3. Mellado, E., Lorenzana, L. M., Rodriguez-Saiz, M., Diez, B., Liras, P., and Barredo, J. L. (2002) The clavulanic acid biosynthetic cluster of *Streptomyces clavuligerus*: genetic organization of the region upstream of the car gene, *Microbiology 148*, 1427−1438.
4. Khaleeli, N., Rongfeng, L., and Townsend, C. A. (1999) Origin of the β-lactam carbons in clavulanic acid from an unusual thiamine pyrophosphate-mediated reaction, *J. Am. Chem. Soc. 121*, 9223−9224.
5. Bachmann, B. O., Li, R., and Townsend, C. A. (1998) beta-Lactam synthetase: a new biosynthetic enzyme, *Proc. Natl. Acad. Sci. U.S.A. 95*, 9082−9086.
6. McNaughton, H. J., Thirkettle, J. E., Zhang, Z., Schofield, C. J., Jensen, S. E., Barton, B., and Greaves, P. (1998) β-lactam synthetase: implications for β-lactamase evolution, *Chem. Commun.* 2325−2326.
7. Wu, T. K., Busby, R. W., Houston, T. A., McIlwaine, D. B., Egan, L. A., and Townsend, C. A. (1995) Identification, cloning, sequencing, and overexpression of the gene encoding proclavaminate amidino hydrolase and characterization of protein function in clavulanic acid biosynthesis, *J. Bacteriol. 177*, 3714−3720.
8. Elson, S. W., Baggaley, K. H., Gillett, J., Holland, S., Nicholson, N. H., Sime, J. T., and Woroniecki, S. R. (1987) Isolation of two novel intracellular β-lactams and a novel dioxygenase cyclising enzyme from *Streptomyces clavuligerus*, *J. Chem. Soc., Chem. Commun.* 1736−1738.
9. Baldwin, J. E., Adlington, R. M., Bryans, J. S., Bringhen, A. O., Coates, J. B., Crouch, N. P., Lloyd, M. D., Schofield, C. J., Elson, S. W., Baggaley, K. H., Cassells, R., and Nicholson, N. H. (1990) Isolation of an intermediate in clavulanic acid biosynthesis, *J. Chem. Soc., Chem. Commun.* 617−619.
10. Marsh, E. N., Chang, M. D., and Townsend, C. A. (1992) Two isozymes of clavaminate synthase central to clavulanic acid formation: cloning and sequencing of both genes from *Streptomyces clavuligerus*, *Biochemistry 31*, 12648−12657.
11. Salowe, S. P., Marsh, E. N., and Townsend, C. A. (1990) Purification and characterization of clavaminate synthase from *Streptomyces clavuligerus*: an unusual oxidative enzyme in natural product biosynthesis, *Biochemistry 29*, 6499−6508.

12. Caines, M. E., Elkins, J. M., Hewitson, K. S., and Schofield, C. J. (2004) Crystal structure and mechanistic implications of N^2-(2-carboxyethyl)arginine synthase, the first enzyme in the clavulanic acid biosynthesis pathway, *J. Biol. Chem. 279*, 5685−5692.
13. Miller, M. T., Bachmann, B. O., Townsend, C. A., and Rosenzweig, A. C. (2001) Structure of beta-lactam synthetase reveals how to synthesize antibiotics instead of asparagine, *Nat. Struct. Biol. 8*, 684−689.
14. Zhang, Z., Ren, J., Stammers, D. K., Baldwin, J. E., Harlos, K., and Schofield, C. J. (2000) Structural origins of the selectivity of the trifunctional oxygenase clavaminic acid synthase, *Nat. Struct. Biol. 7*, 127−133.
15. Elkins, J. M., Clifton, I. J., Hernandez, H., Doan, L. X., Robinson, C. V., Schofield, C. J., and Hewitson, K. S. (2002) Oligomeric structure of proclavaminic acid amidino hydrolase: evolution of a hydrolytic enzyme in clavulanic acid biosynthesis, *Biochem. J. 366*, 423−434.
16. Elkins, J. M., Kershaw, N. J., and Schofield, C. J. (2005) X-ray crystal structure of ornithine acetyltransferase from the clavulanic acid biosynthesis gene cluster, *Biochem. J. 385*, 565−573.
17. Arulanantham, H., Kershaw, N. J., Hewitson, K. S., Hughes, C. E., Thirkettle, J. E., and Schofield, C. J. (2006) ORF17 from the clavulanic acid biosynthesis gene cluster catalyzes the ATP-dependent formation of N-glycyl-clavaminic acid, *J. Biol. Chem. 281*, 279−287.
18. Egan, L. A., Busby, R. W., Iwata-Reuyl, D., and Townsend, C. A. (1997) Probable role of clavaminic acid as the terminal intermediate in the common pathway to clavulanic acid and the antipodal clavam metabolites, *J. Am. Chem. Soc. 119*, 2348−2355.
19. Nicholson, N. H., Baggaley, K. H., Cassells, R., Elson, S. W., Fulston, M., Tyler, J. W., and Woroniecki, S. R. (1994) Evidence that the immediate biosynthetic precursor of clavulanic acid is its N-aldehyde analogue, *J. Chem. Soc., Chem. Commun.* 1281−1282.
20. Fulston, M., Davison, M., Elson, S. W., Nicholson, N. H., Tyler, J. W., and Woroniecki, S. R. (2001) Clavulanic acid biosynthesis; the final steps, *J. Chem. Soc., Perkin Trans. 1*, 1122−1130.
21. Otwinowski, Z., and Minor, W. (1997) Processing of X-ray diffraction data collected in oscillation mode, *Methods Enzymol. 276*, 307−326.
22. Collaborative Computational Project, Number 4 (1994) The CCP4 suite: programs for protein crystallography, *Acta Crystallogr., Sect. D 50*, 760−763.
23. Leslie, A. G. W. (1992) Recent changes to the MOSFLM package for processing film and image plate data, *Joint CCP4 + ESF-EAMCB Newsletter on Protein Crystallography, No. 26*.
24. Matthews, B. W. (1968) Solvent content of protein crystals, *J. Mol. Biol. 33*, 491−497.
25. Schneider, T. R., and Sheldrick, G. M. (2002) Substructure solution with SHELXD, *Acta Crystallogr., Sect. D 58*, 1772−1779.
26. La Fortelle, E., and Bricogne, G. (1997) Maximum-likelihood heavy-atom parameter refinement for the multiple isomorphous replacement and multiwavelength anomalous diffraction methods, in *Methods Enzymol. 276*, 472−492.
27. Abrahams, J. P., and Leslie, A. G. (1996) Methods used in the structure determination of bovine mitochondrial F1 ATPase, *Acta Crystallogr., Sect. D 52*, 30−42.
28. Perrakis, A., Morris, R., and Lamzin, V. S. (1999) Automated protein model building combined with iterative structure refinement, *Nat. Struct. Biol. 6*, 458−463.
29. Yang, J. K., Park, M. S., Waldo, G. S., and Suh, S. W. (2003) Directed evolution approach to a structural genomics project: Rv2002 from *Mycobacterium tuberculosis*, *Proc. Natl. Acad. Sci. U.S.A. 100*, 455−460.
30. Kleywegt, G. J., and Read, R. J. (1997) Not your average density, *Structure 5*, 1557−1569.
31. Jones, T. A., Zou, J. Y., Cowan, S. W., and Kjeldgaard, M. (1991) Improved methods for building protein models in electron density maps and the location of errors in these models, *Acta Crystallogr., Sect. A 47*, 110−119.
32. Brunger, A. T., Adams, P. D., Clore, G. M., DeLano, W. L., Gros, P., Grosse-Kunstleve, R. W., Jiang, J. S., Kuszewski, J., Nilges, M., Pannu, N. S., Read, R. J., Rice, L. M., Simonson, T., and Warren, G. L. (1998) Crystallography & NMR system: A new software suite for macromolecular structure determination, *Acta Crystallogr., Sect. D 54*, 905−921.
33. Murshudov, G. N., Vagin, A. A., and Dodson, E. J. (1997) Refinement of macromolecular structures by the maximum-likelihood method, *Acta Crystallogr., Sect. D 53*, 240−255.
34. Winn, M. D., Isupov, M. N., and Murshudov, G. N. (2001) Use of TLS parameters to model anisotropic displacements in macromolecular refinement, *Acta Crystallogr., Sect. D 57*, 122−133.
35. Lamzin, V. S., Perrakis, A., and Wilson, K. S. (2001) The ARP/WARP Suite for Automated Construction and Refinement of Protein Models, in *International Tables for Crystallography. Crystallography of Biological Macromolecules* (Rossmann, M. G., and Arnold, E., Eds.) Vol. F, pp 720−722, Kluwer Academic Publishers, Dordrecht, The Netherlands.
36. Allen, F. H. (2002) The Cambridge structural database: a quarter of a million crystal structures and rising, *Acta Crystallogr., Sect. B 58*, 380−388.
37. Kleywegt, G. J., Henrick, K., Dodson, E. J., and van Aalten, D. M. (2003) Pound-wise but penny-foolish: How well do micromolecules fare in macromolecular refinement? *Structure 11*, 1051−1059.
38. DeLano, W. L. (2002) The PyMOL User's Manual, *User's Manual*, DeLano Scientific, San Carlos, CA.
39. Sobott, F., Hernandez, H., McCammon, M. G., Tito, M. A., and Robinson, C. V. (2002) A tandem mass spectrometer for improved transmission and analysis of large macromolecular assemblies, *Anal. Chem. 74*, 1402−1407.
40. Perez-Redondo, R., Rodriguez-Garcia, A., Martin, J. F., and Liras, P. (1998) The claR gene of *Streptomyces clavuligerus*, encoding a LysR-type regulatory protein controlling clavulanic acid biosynthesis, is linked to the clavulanate-9-aldehyde reductase (car) gene, *Gene 211*, 311−321.
41. Rossmann, M. G., Moras, D., and Olsen, K. W. (1974) Chemical and biological evolution of nucleotide-binding protein, *Nature 250*, 194−199.
42. Rossmann, M. G., Adams, M. J., Buehner, M., Ford, G. C., Hackert, M. L., Liljas, A., Rao, S. T., Banaszak, L. J., Hill, E., Tsernoglou, D., and Webb, L. (1973) Molecular symmetry axes and subunit interfaces in certain dehydrogenases, *J. Mol. Biol. 76*, 533−537.
43. Ghosh, D., Wawrzak, Z., Weeks, C. M., Duax, W. L., and Erman, M. (1994) The refined three-dimensional structure of 3 alpha,20 beta-hydroxysteroid dehydrogenase and possible roles of the residues conserved in short-chain dehydrogenases, *Structure 2*, 629−640.
44. Fisher, M., Kroon, J. T., Martindale, W., Stuitje, A. R., Slabas, A. R., and Rafferty, J. B. (2000) The X-ray structure of *Brassica napus* beta-keto acyl carrier protein reductase and its implications for substrate binding and catalysis, *Structure 8*, 339−347.
45. Otagiri, M., Kurisu, G., Ui, S., Takusagawa, Y., Ohkuma, M., Kudo, T., and Kusunoki, M. (2001) Crystal structure of meso-2,3-butanediol dehydrogenase in a complex with NAD^+ and inhibitor mercaptoethanol at 1.7 Å resolution for understanding of chiral substrate recognition mechanisms, *J. Biochem. (Tokyo) 129*, 205−208.
46. Duax, W. L., Griffin, J. F., and Ghosh, D. (1996) The fascinating complexities of steroid-binding enzymes, *Curr. Opin. Struct. Biol. 6*, 813−823.
47. Tanaka, N., Nonaka, T., Nakamura, K., and Hara, A. (2001) SDR: structure, mechanism of action, and substrate recognition, *Curr. Org. Chem. 5*, 89−111.
48. Filling, C., Berndt, K. D., Benach, J., Knapp, S., Prozorovski, T., Nordling, E., Ladenstein, R., Jörnvall, H., and Oppermann, U. (2002) Critical residues for structure and catalysis in short-chain dehydrogenases/reductases, *J. Biol. Chem. 277*, 25677−25684.
49. Jörnvall, H., Persson, B., Krook, M., Atrian, S., Gonzalez-Duarte, R., Jeffery, J., and Ghosh, D. (1995) Short-chain dehydrogenases/reductases (SDR), *Biochemistry 34*, 6003−6013.
50. Oppermann, U., Filling, C., Hult, M., Shafqat, N., Wu, X., Lindh, M., Shafqat, J., Nordling, E., Kallberg, Y., Persson, B., and Jörnvall, H. (2003) Short-chain dehydrogenases/reductases (SDR): the 2002 update, *Chem.-Biol. Interact. 143−144*, 247−253.
51. Bottoms, C. A., Smith, P. E., and Tanner, J. J. (2002) A structurally conserved water molecule in Rossmann dinucleotide-binding domains, *Protein Sci. 11*, 2125−2137.
52. Kallberg, Y., Oppermann, U., Jörnvall, H., and Persson, B. (2002) Short-chain dehydrogenases/reductases (SDRs), *Eur. J. Biochem. 269*, 4409−4417.
53. Rossmann, M. G., Liljas, A., Brändén, C., and Banaszak, L. J. (1975) Evolutionary and Structural Relationships among Dehydrogenases, *The Enzymes*, Vol. 11, pp 61−101, Academic Press, New York.

54. Chen, Z., Jiang, J. C., Lin, Z. G., Lee, W. R., Baker, M. E., and Chang, S. H. (1993) Site-specific mutagenesis of *Drosophila* alcohol dehydrogenase: evidence for involvement of tyrosine-152 and lysine-156 in catalysis, *Biochemistry 32*, 3342−3346.
55. Tanaka, N., Nonaka, T., Tanabe, T., Yoshimoto, T., Tsuru, D., and Mitsui, Y. (1996) Crystal structures of the binary and ternary complexes of 7 alpha-hydroxysteroid dehydrogenase from *Escherichia coli*, *Biochemistry 35*, 7715−7730.
56. Miller, M. T., Bachmann, B. O., Townsend, C. A., and Rosenzweig, A. C. (2002) The catalytic cycle of beta-lactam synthetase observed by x-ray crystallographic snapshots, *Proc. Natl. Acad. Sci. U.S.A. 99*, 14752−14757.
57. Brown, A. G., Corbett, D. F., Goodacre, J., Harbridge, J. B., Howarth, T. T., Ponsford, R. J., Stirling, I., and King, T. J. (1984) Clavulanic acid and its derivatives. Structure elucidation of clavulanic acid and the preparation of dihydroclavulanic acid, isoclavulanic acid, esters and related oxidation products, *J. Chem. Soc., Perkin Trans. 1*, 635−650.
58. Howarth, T. T., Brown, A. G., and King., T. J. (1976) Clavulanic acid, a novel β-lactam isolated from *Streptomyces clavuligerus*; X-ray crystal structure analysis, *J. Chem. Soc., Chem. Commun.* 266−267.
59. Townsend, C. A., Ho, M.-F., and Mao, S.-S. (1986) The stereochemical fate of (2*RS*,5*R*) and (2*RS*,5*S*)-[5-^{3}H]ornithine in clavulanic acid biosynthesis, *J. Chem. Soc., Chem. Commun.* 638−639.
60. Diederichs, K., and Karplus, P. A. (1997) Improved R-factors for diffraction data analysis in macromolecular crystallography, *Nat. Struct. Biol. 4*, 269−275.
61. Kleywegt, G. J., and Jones, T. A. (1996) Phi/psi-chology: Ramachandran revisited, *Structure 4*, 1395−1400.

BI061978X